Journal of
*Marine Science and Engineering*

MDPI

*Article*

# Experimental Investigation into the Erosion Performance of Water Jets on Marine Hydrate-Bearing Sediment

**Dongbin Pan [1], Lin Yang [2,*], Chen Chen [3,4,*] and Xitong Li [3,4]**

[1] College of Resources and Environmental Engineering, Jiangxi University of Science and Technology, Ganzhou 341000, China
[2] Gas Hydrate Engineering Technology Center, China Geological Survey, Guangzhou Marine Geological Survey, Guangzhou 510075, China
[3] College of Construction Engineering, National Geophysical Exploration Equipment Engineering Research Center, Jilin University, Changchun 130026, China
[4] Key Laboratory of Drilling and Exploitation Technology in Complex Conditions, Ministry of Natural Resources, Changchun 130026, China
* Correspondence: yl_gmgs@163.com (L.Y.); chenchen@jlu.edu.cn (C.C.)

**Abstract:** Fine-grained natural gas hydrate (NGH) reservoirs are widely distributed across the world and bear more than 90% of global NGH. However, it is difficult to exploit this kind of NGH reservoir economically and environmentally using conventional methods. Water-jet cutting is an efficient and environmentally friendly technique for mining such hydrate reservoirs, as the production process does not depend on mass and heat transfer within the formations. In this work, a series of physical experiments were conducted to clarify the erosion performance of marine hydrate-bearing sediment (HBS) impacted by water jets. The results show that the accumulation of sediment particles and hydrate particles at the bottom of erosion hole severely inhibits the vertical erosion of HBS by water jet. For a particular jet flow rate, the jet distance has an optimal value, which is between 4 mm and 28 mm. Moreover, the upwelling flow containing solid particles has a significant impact on the erosion of the hole top. In reservoirs with a low hydrate saturation (20–40%) and reservoirs with a high hydrate saturation (60–80%), the erosion holes exhibit a gourd shape and a bamboo shape, respectively. In addition, the volume erosion efficiency and the depth erosion efficiency are more sensitive to the variation in jet flow rate than jet distance and hydrate saturation. This study can provide theoretical and technical support for the application of water-jet cutting in the exploitation of marine HBS.

**Keywords:** hydrate-bearing sediment; hydrate exploitation technology; water jet; erosion performance

check for updates

**Citation:** Pan, D.; Yang, L.; Chen, C.; Li, X. Experimental Investigation into the Erosion Performance of Water Jets on Marine Hydrate-Bearing Sediment. *J. Mar. Sci. Eng.* **2023**, *11*, 228. https://doi.org/10.3390/jmse11010228

Received: 22 December 2022
Revised: 10 January 2023
Accepted: 12 January 2023
Published: 16 January 2023



## 1. Introduction

Natural gas hydrate (NGH) is solid, crystalline compound formed under certain temperature and pressure conditions, also known as "combustible ice" [1]. NGH is a new energy resource with great development potential [2–4]. Approximately 90% of offshore areas have suitable temperature and pressure conditions for NGH formation and stability. Very clean natural gas can be produced from NGH deposits, especially from submarine hydrate reservoirs [5–7]. It is estimated that natural gas reserves in offshore areas are approximately $2 \times 10^{16}$ $m^3$ [8]. However, the existing marine-NGH exploitation technology is still not mature enough, especially for fine-grained hydrate reservoirs (mainly including clay, sandy, and clayey silt sediments) with low permeability and a weak cementation strength characteristic, which also restricts the commercial development of NGH [9–11].

Early laboratory experiments and production tests indicated that a number of methods could promote the in situ dissociation of NGH and exploit natural gas from NGH [7,12–15]. Moreover, depressurization will be the ideal method to use [16,17]. However, marine NGH mainly occurs in fine-grained sediments [18] and the reservoirs are characterized by a shallow burial depth, lack of dense caprocks, weak cementation, fragility, and low permeability [19–22]. There are some deficiencies in the exploitation of marine NGHs by existing methods. For the depressurization method, Oyama et al. [23] and Konno et al. [24] used depressurization to analyze the dissociation process of methane hydrate in low-permeability sediment. The results showed that pressure drops transfer slowly in the hydrate sediment, and the hydrate dissociates almost exclusively at the contact surface of the decomposition front. Zhong et al. [25] used a numerical simulation method to obtain a similar conclusion. On the aspect of thermal stimulation, Wang et al. [26], Zhao et al. [27], and Selim and Sloan [28] used the thermal stimulation method to analyze the relationship between the dissociation rate and the characteristics of the hydrate sediment. They found that hydrate dissociation would be inhibited in low-permeability conditions. For the carbon dioxide replacement method, Yuan et al. [29], Yang et al. [30], and Chen et al. [31] analyzed the carbon dioxide replacement mechanism of methane hydrate in sediments. The results showed that the replacement efficiency is mainly controlled by the diffusion rate in the deferred reaction stage, and the replacement rate is slow in low-permeability sediment. Thus, the low permeability of hydrate-bearing sediment (HBS) is an urgent problem to be solved for NGH production [32–34].

In 2017, the first offshore natural-gas-hydrate production test was successfully carried out in the Shenhu Area of the South China Sea. For the first time, the reservoir stimulation techniques were used for marine-hydrate production, with a total gas recovery of $3 \times 10^5$ m$^3$ within 60 days [35]. It was shown that reservoir stimulation is an essential technique for NGH production. Zhou et al. [36] presented the solid fluidization method to exploit marine hydrates with low permeability, weak cementation, and unconsolidated formation characteristics. The hydrate trail-production results indicate that the water jet can cut hydrate-bearing sediment effectively. Furthermore, water-jet cutting is also a common and mature formation stimulation technique for increasing the production of low-permeability gas and oil reservoirs [37,38]. Based on the low permeability, weak cementation strength, and unconsolidated formation characteristics of fine-grained marine NGH reservoir, the water-jet cutting technique is also beneficial for increasing the gas and liquid transfer channel, improving the reservoir permeability of the near-wellbore area and increasing the production efficiency of marine NGH.

Currently, few studies have been performed on the erosion performance of water jets on hydrate-bearing sediment (HBS). Wang et al. [39] experimentally investigated the influence of jet flow rate and traverse speed on the erosion efficiency and erosion effect on HBS. They observed that the erosion efficiency increases with increasing traverse speed, while the increase in jet flow rate increases the peak concentration of the solid phase and thus increases the risk of pipeline transport. Tang et al. [40] designed a straight-rotating, mixed nozzle and experimentally investigated the effect of the number of nozzles and structural parameters on erosion efficiency. Wang et al. [41] experimentally researched the critical erosion velocities of water jets for HBS at different hydrate saturations. The results show that the critical velocities for HBS vary in the range of 5.71–10.85 m/s. However, the research targets of the above work were frozen sand soils. In nature, HBS is formed by particles and hydrates filled in a pore space through cementation force. The structure and physical properties of HBS are different from frozen sand soils. Therefore, the performance of water-jet erosion on HBS may be different when compared to that of frozen sand soils. In our previous work [42], an HBS simulation model with the (Arbitrary Lagrangian–Eulerian) ALE method was established, and the influence of nozzle diameter, jet flow rate, and jet distance on erosion performance was explored. The results indicated that an increase in nozzle diameter and jet flow rate could enhance the erosion efficiency of HBS, while an increase in jet distance was detrimental to it. Zhang et al. [43] also numerically investigated the jet-erosion process of HBS by the ALE method. They found that the erosion of HBS by swirling jets was stronger than the erosion by conical jets. However, the HBS models established in the above work were all finite-element models, and the numerical calculation methods ignored the effect of detached particles on jet-erosion behavior and erosion-hole development. In general, the research on the water-jet erosion of HBS is limited at present, and it is necessary to conduct a systematic and in-depth study on the water-jet erosion performance of HBS.

In this work, a physical experiment to clarify the erosion process of HBS impacted by water jets was performed. The influence of the water-jet parameters (jet flow rate and jet distance) and the hydrate saturation on the erosion performances (including erosion volume, erosion depth, erosion-hole top diameter, and erosion-hole bottom diameter) of HBS were investigated extensively. Moreover, the sensitivity of erosion efficiency to these parameters was analyzed.

## 2. Experimental

### 2.1. Materials and Experimental Apparatus

The thermophysical and mechanical properties of tetrahydrofuran (THF) hydrate and $CH_4$ hydrate are similar [44–46]. In contrast, the former can exist stably at an ambient temperature of 4 °C and a pressure of 0.1 MPa, and it has the characteristics of rapid formation and uniform distribution [44–46]. Therefore, in this work, THF was used to prepare HBS samples to ensure the operational simplicity and safety of water-jet erosion experiments. THF (99.99% purity) was supplied by the Changzhou Tongxiang Chemical Corporation in China. The water was distilled and deionized. The HBS samples were formed from silica sands (20–40 mesh sizes), and the THF solution with a mass fraction of 19%.

A schematic of the experimental apparatus used in this work is shown in Figure 1. The experimental apparatus mainly consisted of a high-pressure reactor, a jet nozzle, a water bath, a jet flow pump, a constant-flux pump, a data acquisition and control system, a back-pressure system, and a solid–liquid separation device. The high-pressure reactor with an effective size of 82 mm × 82 mm × 150 mm is made of 316L stainless steel, and the maximum working pressure is 20 MPa. The jet flow pump can be adjusted without steps, and the range of the jet flow is 0–2500 mL/min. The jet flow erosion experiment of different jet distances could be realized by adjusting the jet-nozzle position. The adjustable range of jet distance is 0–40 mm. The water bath was used to control the experimental temperature. Two temperature probes were inserted into sediments at vertical distances to the inner top of the reactor of 40 mm and 80 mm, respectively. A pressure sensor was fixed on the middle position of the reactor. The uncertainties of pressure and temperature measurement were ±25 KPa and ±0.1 °C, respectively. The back pressure system was composed of a hand pump, a buffer container, and a back pressure valve, and it was used to control the outlet pressure of the solid–liquid mixture generated by the jet erosion of HBS. The pressure fluid was supplied by the constant-flux pump. The piston in the reactor could move under the push of the pressure liquid, thus compacting sediments. The data acquisition and control system was mainly used to record temperature and pressure data as well as to control the process of water jet erosion.

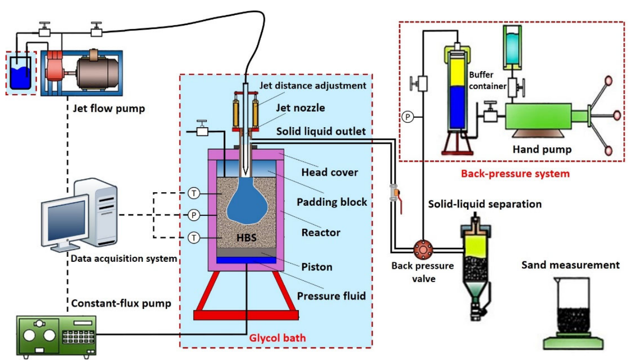


**Figure 1.** Schematic of the experimental apparatus.

### 2.2. Procedures

#### 2.2.1. Hydrate Formation in Sediments

A THF solution with a mass fraction of 19% was prepared, which is suitable for THF-hydrate formation [47–49]. The 19% mass fraction ensured that the THF and water could be completely consumed simultaneously during the formation of hydrate [47]. A certain amount of THF solution was mixed well with the dried quartz sand in a closed vessel. Then, the prepared sediment specimen was quickly loaded into the reactor. The padding block, the head cover, and the jet nozzle were installed. Afterwards, a specific amount of pressure fluid was pumped into the reactor by the constant-flux pump. The piston moved upwards to compress the sample, controlling its height to 130 mm. In all experiments, the length, width, and height of the specimens were 82 mm, 82 mm, and 130 mm, respectively. In each specimen, the actual volume of silica sand and the porosity were 611.9 $cm^3$ and 30%, respectively. Finally, the reactor was put into the water bath, and the hydrates were completely formed after maintaining the formation temperature at −9 °C for 48 h [47–49].

#### 2.2.2. Water-Jet Erosion

After hydrate formation, the water bath temperature was regulated to 1 °C. The jet distance (defined as the vertical distance from the jet start position to the HBS surface) was adjusted to a predetermined value after the reactor temperature and the supply water temperature of the jet flow pump were stabilized at the temperature value. It was calculated from the point of exit of the water from the nozzle. The nozzle diameter was 1 mm in all experiments. To simplify the experimental procedure, the outlet pressure (back pressure) of the solid–liquid mixture was set to 0 in this work. The jet flow rate was then set, and the experiment of eroding the hydrate sediment by water jet was carried out. The duration of the experiment was 30 s. After jet erosion, the reactor was transferred to a low-temperature chamber (ambient temperature of 1 °C), and the residual liquid and sand in the erosion hole were removed. The total mass of erosion particles after being dried was measured, and the erosion-hole parameters were measured using a vernier caliper. The measurement error of the vernier caliper was ±0.03 mm/150 mm. The measured parameters included the depth of erosion, the diameter of the hole at different depths in the selected section, the maximum diameter of the erosion-hole top, and the maximum diameter of the erosion-hole bottom. Table 1 illustrates the experimental conditions for the water-jet erosion of HBS. Based on the experimental equipment conditions, the water-jet flow rates were selected as 1100–2000 mL/min.

**Table 1.** Experimental conditions for water jet erosion of HBS.

| Runs | Jet Flow Rate (mL/min) | Jet Distance (mm) | Hydrate Saturation (%) | Porosity (%) |
|---|---|---|---|---|
| 1 | 1100 | 15 | 50 | 30 |
| 2 | 1400 | 15 | 50 | 30 |
| 3 | 1700 | 15 | 50 | 30 |
| 4 | 2000 | 15 | 50 | 30 |
| 5 | 1700 | 4 | 50 | 30 |
| 6 | 1700 | 16 | 50 | 30 |
| 7 | 1700 | 28 | 50 | 30 |
| 8 | 1700 | 40 | 50 | 30 |
| 9 | 1700 | 15 | 20 | 30 |
| 10 | 1700 | 15 | 40 | 30 |
| 11 | 1700 | 15 | 60 | 30 |
| 12 | 1700 | 15 | 80 | 30 |

### 2.3. Calculations

In this work, the erosion volume after water-jet erosion of HBS can be calculated as follows:

$$V_{erosion} = \frac{m_s \cdot V_s}{m_{total}} \tag{1}$$

$$m_{total} = \rho_s \cdot [V_s(1 - \Phi)] \tag{2}$$

where $m_s$ is the total mass of erosion particles after being dried and $V_s$ is the volume of hydrate sediment specimens, which was $8.2 \times 8.2 \times 13 = 874.12\ \text{cm}^3$. $m_{total}$ is the total mass of sand loaded into the reactor, $\rho_s$ is the particle density of the quartz sand, and $\Phi$ is the porosity.

A THF solution with a mass fraction of 19% was used. The volume of THF, $V_{THF}$,and the distilled water, $V_w$, can be calculated by Equations (3) and (4).

$$V_{THF} + V_w = \Phi V_s S_{hyd} \tag{3}$$

$$\frac{\rho_{THF} V_{THF}}{\rho_{THF} V_{THF} + \rho_w V_w} = 19\% \tag{4}$$

where $S_{hyd}$ is the hydrate saturation of hydrate sediment specimens and $\rho_{THF}$ and $\rho_w$ are the density of THF and distilled water, respectively.

## 3. Results and Discussion

### 3.1. The Influence Rules of Jet Flow Rate on Erosion Performance

In this section, four tests were conducted to research the influence rules of jet flow rate on erosion performance. The jet flow rates used were in the range of 1100 mL/min to 2000 mL/min. A jet distance of 15 mm was used, and the hydrate saturation of the HBS was 50%. Given that the erosion holes in these runs had similar morphologies, the erosion-hole section of Run 3 were used for illustration.

Figure 2 shows the influence of jet flow rate on erosion volume and the scatter plot of the erosion-hole section of Run 3. An increase in jet flow rate corresponds to an increase in erosion volume, and the erosion volume increases rapidly at a high flow rate. When comparing Run 1 and Run 2, Run 2 and Run 3, and Run 3 and Run 4, the erosion volume increased by 48.1%, 52.7%, and 53.0%, respectively. This result indicates that the higher the jet flow rate, the higher the jet erosion efficiency of HBS. This phenomenon should be related to the erosion characteristics of the jet fluid on HBS. In HBS, hydrate has a cementing and supporting effect on sediment particles [45,46]. The erosion of HBS under the action of jet fluid is essentially the process of detaching sediment particles and hydrate particles. The erosion process of HBS is shown in Figure 3. In the early stage (Figure 3a), the penetration range of the jet fluid in HBS is small, and the water jet mainly causes the detachment of particles in the vertical direction (vertical erosion). The fluid flow in the erosion hole returns up the hole wall and has a stripping effect on the solid particles contacted along the way, i.e., radial erosion occurs. In the later stage (Figure 3b), the penetration range of the jet fluid in HBS increases, and the depth of the erosion hole increases. Moreover, the pore-fluid pressure of HBS around the erosion hole increases, resulting in a decrease in the effective stress. As a result, the solid particles on the wall of the erosion hole are more easily stripped by the upward return-fluid flow, and the hole extends rapidly in the radial direction. Therefore, a gourd-like erosion hole is formed in HBS at the end of jet erosion. Hence, the increase in jet flow rate can enhance the erosion efficiency of volume.

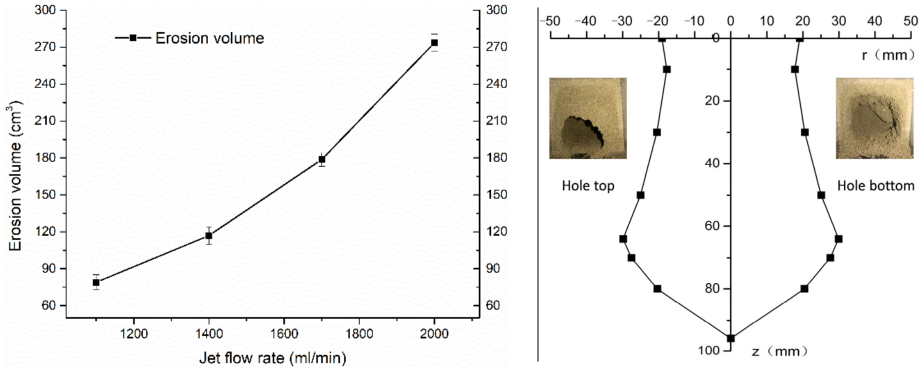


**Figure 2.** The influence of jet flow rate on erosion volume and the scatter plot of the erosion-hole section of Run 3.

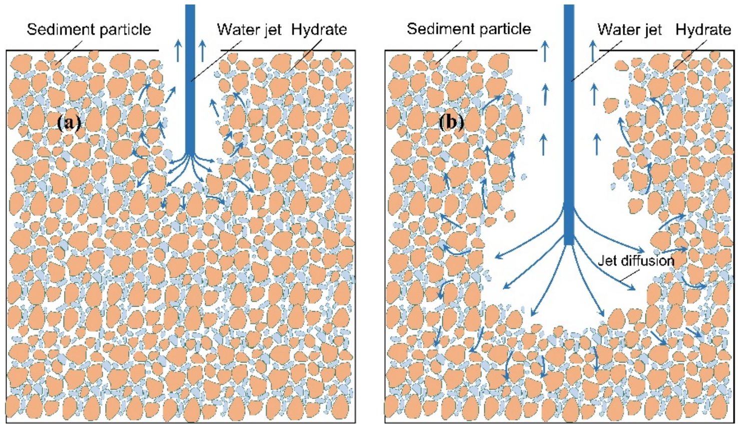


**Figure 3.** The water-jet erosion process of HBS: (**a**) the early stage of erosion; (**b**) the later stage of erosion.

Figure 4 illustrates the influence of the jet flow rate on erosion depth, the maximum diameter of the erosion-hole top, and the maximum diameter of the erosion-hole bottom. The evolution of the maximum diameters of the erosion-hole top and erosion-hole bottom is similar to that of the erosion volume; they increase more rapidly at a higher flow rate. This is understandable given that the increase in jet flow can increase the radial erosion intensity. However, it should be noted that the evolution of erosion depth is different from that of erosion volume. The growth rate of erosion depth decreases with an increasing jet flow rate. This result indicates that the enhancement of the vertical erosion degree of HBS at high jet flow is limited. Combined with the evolution of erosion volume in Figure 2, it can be considered that the increase in erosion volume is mainly contributed to by the radial erosion of HBS. This phenomenon is caused by the accumulation of stripped sediment particles at the bottom of the erosion hole, which is observed in all experimental runs. Although the increased jet flow rate increases erosion volume, the amount of stripped particles that are not discharged from the erosion hole also increases. Inevitably, the number of free particles deposited to the bottom of the erosion hole also increases. These free particles severely inhibit the vertical erosion of HBS by water jet. In our previous numerical simulation study of water-jet erosion of HBS [42], the erosion depth increased linearly with increasing jet flow, which differs from the results in this work. This may be due to the material model of HBS. The material model in the previous study was a finite-element model, and there was no free-particle accumulation at the bottom of the erosion hole.

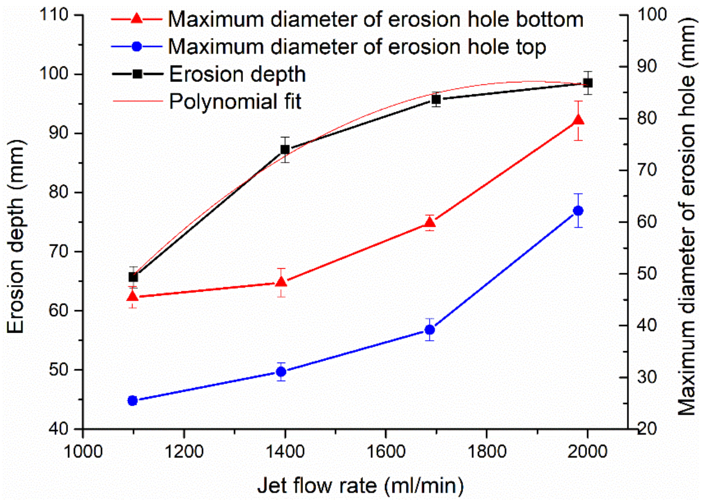


**Figure 4.** The influence of jet flow rate on the erosion depth, the maximum diameter of the erosion-hole top, and the maximum diameter of the erosion-hole bottom.

By analyzing the erosion process of rock and frozen soil sediment by jet, it was found that a critical erosion velocity exists, which means rock and frozen soil sediment is not broken when the jet velocity is less than the critical erosion velocity [41,50]. By analyzing the relationship between the jet velocity and erosion depth within a certain range, a corresponding mathematical expression can be established to analyze the critical erosion velocity of hydrate sediment. Figure 4 illustrates the curve diagram of the corresponding relation between erosion depth and jet flow rate. The erosion depth $L$ ($y$-axis) is a polynomial function of the jet flow rate $Q$ ($x$-axis) when the jet distance is 15 mm and the hydrate saturation is 50%. The fitted-trend equation can be expressed by following relationship:

$$L = -87.41 + 0.197Q - 5.194 \times 10^{-5}Q^2$$

When the erosion depth $L$ = 0, the corresponding jet flow rate is 513.1 mL/min. The diameter of the jet nozzle used in these runs is 1 mm. The corresponding jet velocity at the nozzle outlet is $v_0$ = 10.89 m/s. This means that HBS can only be eroded if the jet velocity at the nozzle exit is greater than this velocity value. As is shown in Figure 5, the structure of the submerged water jet can be divided into the initial segment and the basic segment after exiting the nozzle [51]. The initial segment consists of the core area in which axial velocity is kept the same, and the axial velocity of the basic segment declines with an increase in distance from the nozzle. The axial velocity ($v_x$) can be expressed as Equation (5) [52].

$$v_x/v_0 = \begin{cases} 1 & (s < s_0) \\ 13.2R_0/(s + 4R_0) & (s \geqslant s_0) \end{cases} \tag{5}$$

where $R_0$ is the water jet radius, $s_0$ is the axial length of the initial segment, and $s_0 = 12.6R_0$ [53]. Combining the jet velocity of the nozzle outlet, $v_0$ = 10.89 m/s, with the jet distance, S = 15 mm, in Runs 1–4, the critical erosion velocity of the HBS with a 50% hydrate saturation can be obtained as 4.58 m/s. However, the critical erosion velocity of 5.71–10.85 m/s (corresponding to 20–80% of hydrate saturation) for HBS obtained by Wang et al. [41] is higher than the critical velocity obtained in this work. The difference should be related to the sediment's grain composition. Frozen sand soils were chosen as a substitute for HBS in the work of Wang et al. [41]. The higher content of fine particles (clay particles) in the frozen sand soil results in a more cohesive sample and thus increases the critical erosion velocity. Additionally, the difference in the physicomechanical properties of ice and THF hydrate may also be responsible for this phenomenon.

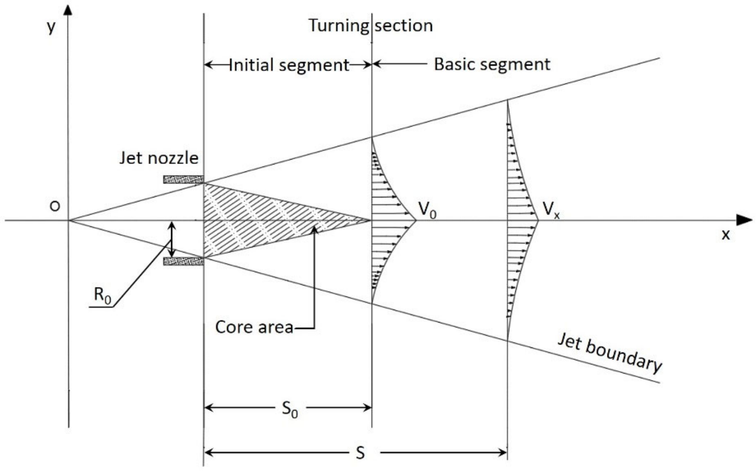


**Figure 5.** The structure of the submerged water jet, modified from Yanaida and Ohashi [51]. $R_0$ is the water jet radius, $s_0$ is the axial length of the initial segment, $s$ is the jet distance, $v_0$ is the jet velocity at the nozzle outlet, and $v_x$ is the axial velocity.

In general, when water jets are used to erode marine hydrate reservoirs in actual mining projects, it is recommended to increase the jet flow rate as much as possible to improve the mining efficiency without exceeding the equipment capacity. Moreover, necessary measures should be taken to facilitate the discharge of solid particles accumulated inside erosion holes to improve the jet's energy utilization efficiency.

### 3.2. The Influence Rules of Jet Distance on Erosion Performance

In this section, four tests were conducted to study the influence rules of jet distance on erosion performance. The jet distances used were in the range of 4 mm to 40 mm. A jet flow rate of 1700 mL/min was used, and the hydrate saturation of the HBS was 50%.

Figure 6 shows the influence of jet distance on erosion volume and erosion depth. As can be seen, the erosion volume is decreased with increasing jet distance, and the reduction rate gradually increases. By comparing Run 5 and Run 6, Run 6 and Run 7, and Run 7 and Run 8, the erosion volume decreased by 7.4%, 19.4%, and 36.5%, respectively. This indicates that there is a higher erosion efficiency when the jet distance is smaller. This observation is caused by jet energy dissipation. The jet fluid continuously exchanges momentum with the surrounding fluid during its motion, thus causing energy dissipation. Moreover, the jet energy dissipation is particularly strong in the submerged state. Therefore, the larger the jet distance, the greater the jet energy dissipation and the lower the erosion efficiency. On the other hand, it is found that the evolution of erosion depth is similar to that of erosion volume. Overall, the erosion depth is also decreased with an increasing jet distance. However, it is important to note that there is an optimal value of jet distance corresponding to the maximum depth of erosion. The optimal jet distance value is between 4 mm and 28 mm. Moreover, the difference in erosion depth is small when the jet distance is less than the optimal value, and the erosion depth decreases rapidly when the jet distance exceeds the optimal value. The analysis suggests that although an appropriate increase in the jet distance reduces the energy carried by the water jet and reduces the erosion volume, the eroded particles that accumulate at the bottom of the erosion hole are also reduced, which creates a favorable environment for vertical erosion. As a result, the erosion depth increases. This factor may be the reason for the emergence of the optimal jet distance. It is generally necessary to find the optimal jet distance in practical engineering, which can maintain a high erosion efficiency and make maximize the erosion depth.

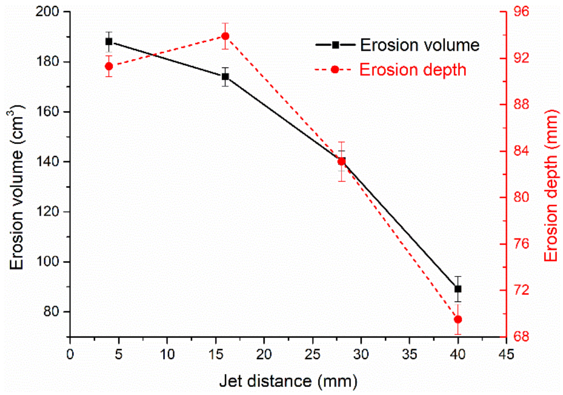


**Figure 6.** The influence of jet distance on erosion volume and erosion depth.

In Figure 7, it can be seen that the maximum diameter of the erosion-hole top decreases slightly with an increase in jet distance. When the jet distance increases from 4 mm to 40 mm, the maximum diameter of the erosion-hole top decreases by 12.7%. This phenomenon should be related to the erosion of the hole top by upwelling flow. As mentioned earlier, the upwelling flow carries a large number of solid particles. These solid-phase components contain both sand particles and hydrate particles. Early studies reported that an increase in the solid-phase content of fluids can enhance their mechanical properties (viscosity and specific weight) and improve the ability of fluids to erode sediments [54,55]. Combined with Figure 6, the increased jet distance significantly reduces erosion volume. As a result, the solid-phase content in the upwelling flow is also reduced, which can reduce its erosion on the top of HBS. Therefore, a higher jet distance corresponds to a smaller diameter of the erosion-hole top. In fact, the water jet is able to continuously absorb the surrounding fluid during its movement and thus diffuse (see Figure 5). Accordingly, an increase in the jet distance can increase the action range of the jet on the HBS surface. However, in combination with the evolution of the maximum diameter of the erosion-hole top, it can be determined that the diffusion of the water jet has less influence on this erosion parameter, and the upwelling flow containing solid particles plays a dominant role in the erosion of the hole top. As for the maximum diameter of the erosion-hole bottom, this decreases with an increase in the jet distance. When the jet distance increases from 4 mm to 40 mm, the maximum diameter of the erosion-hole bottom decreases by 20%. This is understandable considering that the energy carried by the water jet after reaching the bottom of the hole is substantially dissipated, weakening its radial erosion of the HBS. In addition, the maximum diameter of the erosion-hole bottom decreases more than the top. This proves that the effect of the jet distance change on erosion at the bottom of hole is greater than that at the top of the hole.

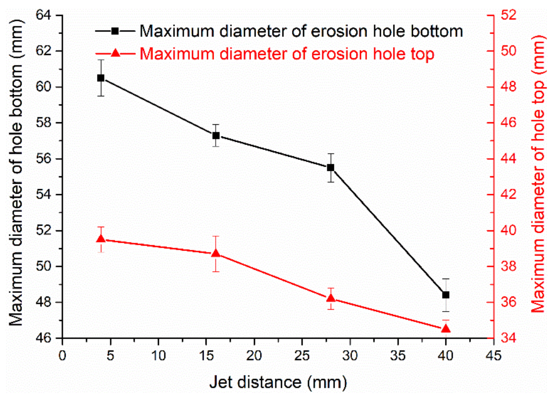


**Figure 7.** The influence of jet distance on the maximum diameter of the erosion-hole top and the maximum diameter of the erosion-hole bottom.

### 3.3. The Influence Rules of Hydrate Saturation on Erosion Performance

In this section, four tests were conducted to investigate the influence rules of hydrate saturation on erosion performance. The hydrate saturations used were in the range of 20% to 80%. The jet flow rate of 1700 cm ml/min was used, and the jet distance was 15 mm.

Figure 8 shows the influence of the hydrate saturation on erosion volume and erosion depth. As shown, the erosion volume is decreased with increasing hydrate saturation, and it decreases more rapidly at a lower hydrate saturation. When the hydrate saturation increases from 20% to 80%, the erosion volume decreases by 64.5%. These phenomena are attributed to the effect of the hydrate saturation on the cementation strength of the sediment particles. At a low hydrate saturation (20–40%), the cementation effect of the hydrate on sediment particles is weak, the interparticle cohesion is low, and the particles are easily stripped under the action of jet fluids. Therefore, low hydrate saturation enhances both vertical and radial erosion of HBS by water jets. This is evidenced by the lower hydrate saturation corresponding to the higher erosion depth and the two larger diameters in Figure 9. Therefore, the erosion efficiency of water jets on HBS is significantly higher in lower hydrate saturation reservoirs. Moreover, it is found that the erosion holes are mainly gourd-shaped at lower hydrate saturations, as illustrated in Figure 10a. On the other hand, under the higher hydrate-saturation conditions (60–80%), the cementation of the hydrate to the sediment particles is stronger, the cohesion between solid particles is greater, and the particles are less likely to be flaked off under the action of jet fluids. Therefore, high hydrate saturation reduces the degree of vertical erosion and radial erosion of HBS by water jets. Hence, the erosion efficiency of water jets is greatly reduced in the high-hydrate-saturation reservoir, and the erosion holes are mainly bamboo-like (as shown in Figure 10b).

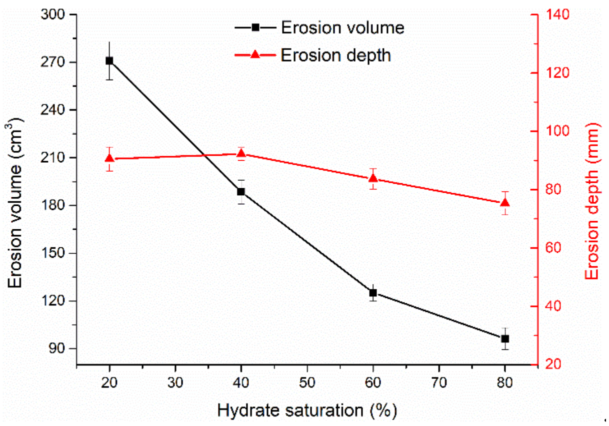


**Figure 8.** The influence of hydrate saturation on erosion volume and erosion depth.

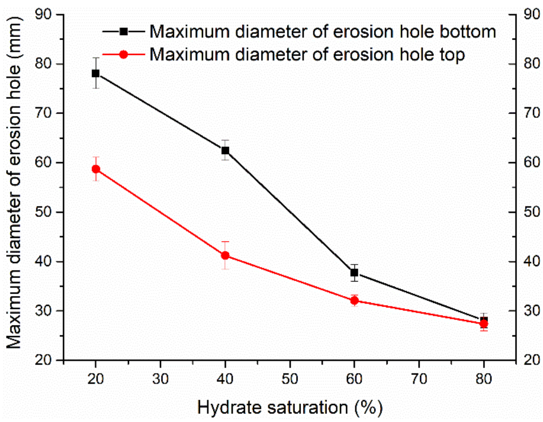


**Figure 9.** The influence of hydrate saturation on the maximum diameter of the erosion-hole top and the maximum diameter of the erosion-hole bottom.

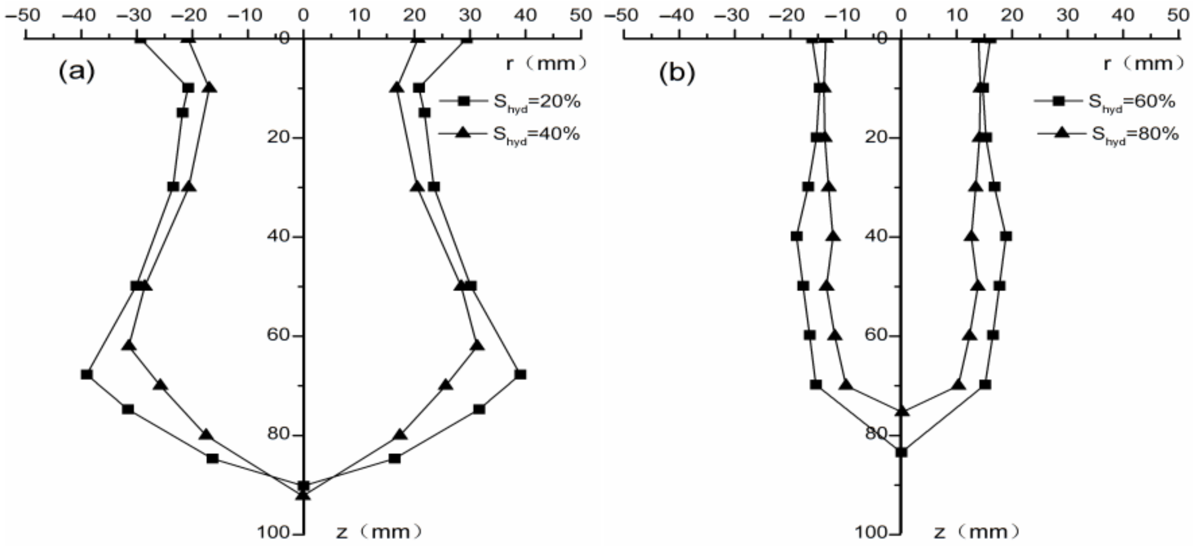


**Figure 10.** Scatter plots of the erosion holes section at different hydrate saturation. (**a**) 20–40%; (**b**) 60–80%.

Regarding the aspect of the erosion depth in Figure 8, the evolutionary process is similar to that of the erosion volume. In comparing Run 9 and Run 12, the erosion depth decreases by 16.8%. It should be noted that, as the hydrate saturation increases, the decrease in erosion depth is slighter than that of the erosion volume. This is attributed to the accumulation of stripped, solid particles at the bottom of the erosion hole. Although the increase in hydrate saturation reduces the degree of vertical erosion of the HBS by water jets, at the same time, the content of solid particles accumulated at the bottom of the hole is reduced. This, to some extent, facilitates the growth of the erosion depth. In Figure 10, it can be seen that the variation trends of the maximum diameter of the erosion-hole top and the maximum diameter of the erosion-hole bottom are also similar to that of the erosion volume. When the hydrate saturation increases from 20% to 80%, the maximum diameter of the erosion-hole top and the maximum diameter of the erosion-hole bottom decrease by 53.3% and 64%, respectively. In addition to the effect of sediment-particle cementation strength on the degree of radial erosion of the HBS, the magnitude of the solid-phase content in the upward fluid flow may be another factor contributing to this result. As the erosion volume increases greatly at a low hydrate saturation, the solid-phase content in the upward flow increases. These upwelling streams can enhance the radial erosion at the top and bottom of the hole. However, it should be noted that the decrease in the diameter of the erosion-hole bottom is higher than that of the hole top. This proves that the effect of hydrate-saturation change on the erosion at the bottom of hole is greater than that at the top.

### 3.4. Sensitivity Analysis of Jet Parameters and Hydrate Saturation on Erosion Efficiency

In this work, the significance of jet flow rate, jet distance, and hydrate saturation on erosion efficiency was comparatively analyzed. The average erosion rate of volume represents the volume erosion efficiency ($\eta_v$) and the average erosion rate of depth represents the depth erosion efficiency ($\eta_d$). Figure 11 illustrates the comparison of the influence of these parameters on erosion efficiencies.

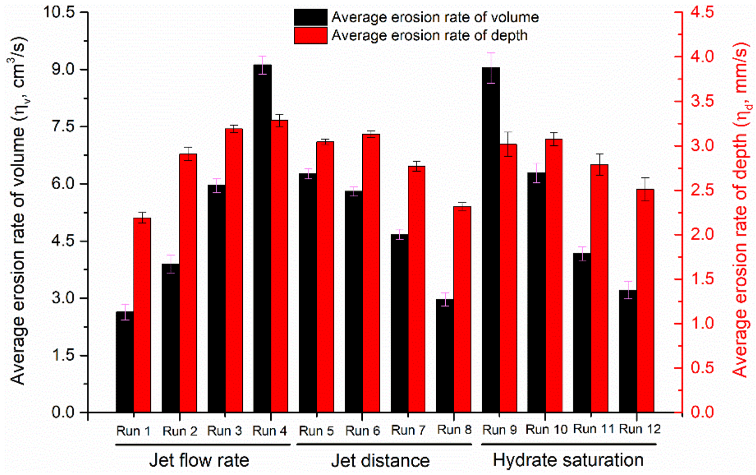


**Figure 11.** The influence of jet parameters and hydrate saturation on the average erosion rate of volume and average erosion rate of depth.

As is shown in Figure 11, the average erosion rate of volume for the jet flow rate is at a minimum in Run 1 and a maximum in Run 4, with the latter being 246% higher than the former. The maximum differences in the average erosion rates of volume for different jet distances and hydrate saturations are 111% and 182%, respectively. This means that the jet flow rate has the most significant influence on volume erosion efficiency, followed by hydrate saturation and then jet distance. In other words, the volume erosion efficiency is most sensitive to the change in jet flow rate, followed by hydrate saturation and then jet distance. Moreover, the effect of the jet flow rate on the volume erosion efficiency is significantly greater than that of the jet distance. Therefore, it can be concluded that, for a specific hydrate saturation reservoir, increasing the jet flow rate is a more suitable way to increase the volume erosion efficiency when compared to adjusting the jet distance during the erosion of the HBS by water jets. On the other hand, the average erosion rate of depth for jet flow rate was the smallest in Run 1 and the highest in Run 4, the latter being 50% higher than the former. The maximum difference in the average erosion rates of depth for different jet distances and hydrate saturations is 31% and 20%, respectively. This result indicates that the depth erosion efficiency is most sensitive to the change in jet velocity, followed by jet distance and then hydrate saturation. Moreover, the effects of jet flow rate and jet distance on the depth erosion efficiency are similar. It can be concluded that changing both the jet velocity and jet distance can effectively regulate erosion depth during water-jet erosion of subsea hydrate reservoirs. In addition, it can be found in Figure 11 that the variation range of the average erosion rate of the depth is remarkably lower than the average erosion rate of the volume. This result indicates that the depth erosion efficiency is significantly less sensitive to the jet parameters and hydrate saturation than the volume erosion efficiency.

## 4. Conclusions

This experiment investigated the influence rules of jet flow rate, jet distance, and hydrate saturation on the erosion effect of hydrate sediments and analyzed the sensitivity of erosion efficiency to these parameters. The main conclusions are as follows.

(1) An increase in the jet flow rate can simultaneously enhance the vertical and radial erosion of HBS and improve the volume erosion efficiency. The accumulation of sediment particles and hydrate particles at the bottom of the erosion hole severely inhibits the vertical erosion of HBS by the water jet. The critical erosion velocity of HBS with a 50% hydrate saturation is 4.58 m/s.

(2) The volume erosion efficiency decreases with an increase in jet distance. For a particular jet flow rate, the jet distance has an optimal value, and the erosion depth decreases rapidly when the jet distance exceeds the optimal value. In this experiment, the opti-

mal jet distance value was between 4 mm and 28 mm. The diffusion of the water jet during its movement has less influence on the maximum diameter of the erosion-hole top, and the upwelling flow containing solid particles plays a dominant role in the erosion of the hole top.

(3) Increasing hydrate saturation can significantly reduce the erosion volume of HBS due to increased cohesion between the sediment particles. At a low hydrate saturation (20–40%), the erosion holes are mainly gourd-shaped. At a high hydrate saturation (60–80%), the erosion depth decreases slightly because fewer particles accumulate in the erosion holes, and the erosion holes are mainly bamboo-shaped.

(4) The volume erosion efficiency is most sensitive to the change in jet velocity, followed by hydrate saturation and then jet distance. The effect of the jet velocity on the volume erosion efficiency is significantly greater than that of the jet distance. Furthermore, the depth erosion efficiency is most sensitive to the change in jet velocity, followed by jet distance and then hydrate saturation. The effects of the jet velocity and jet distance on erosion depth are similar.

Although the erosion performances of water jets on HBS under different jet flow rates, jet distance, and hydrate saturation conditions were obtained, the erosion process of HBS is complex and still needs to be deeply studied. The gas hydrate specimen is beneficial for the study of the erosion effect of marine NGH sediment. Moreover, it is also necessary to consider the pressure and temperature conditions as well as the direction of jet flow are also necessary. Certainly, it still requires more experimental apparatus and experiments to be verified, studies which are currently under consideration.

**Author Contributions:** D.P., methodology, formal analysis, writing—original draft, writing—review & editing; L.Y., conceptualization, data curation; C.C., conceptualization, funding acquisition, project administration; X.L., methodology, formal analysis. All authors have read and agreed to the published version of the manuscript.

**Funding:** This research was funded by the Jiangxi Provincial Natural Science Foundation grant number 20224BAB213044, the Science and Technology Research Project of Jiangxi Provincial Education Department grant number GJJ210863, the National Natural Science Foundation of China grant number 41672361, and the National Special Project on Gas Hydrate of China grant number DD20160217 and DD20160221.

**Institutional Review Board Statement:** Not applicable.

**Informed Consent Statement:** Not applicable.

**Data Availability Statement:** The data presented in this study are available on request from the corresponding author.

**Conflicts of Interest:** The authors declare no conflict of interest.

## References

1. Collett, T. Energy resource potential of natural gas hydrates. *AAPG Bull.* **2002**, *86*, 1971–1992.
2. Max, M.; Johnson, A. *Exploration and Production of Oceanic Natural Gas Hydrate: Critical Factors for Commercialization*; Springer: Basel, Switzerland, 2016; p. 405.
3. Yoneda, J.; Oshima, M.; Kida, M.; Kato, A.; Konno, Y.; Jin, Y.; Jang, J.; Waite, W.F.; Kumar, P.; Tenma, N. Pressure core based onshore laboratory analysis on mechanical properties of hydrate-bearing sediments recovered during India's National Gas Hydrate Program Expedition (NGHP) 02. *Mar. Pet. Geol.* **2018**, *108*, 482–501. [CrossRef]
4. Makogon, Y.F. Natural gas hydrates—A promising source of energy. *J. Nat. Gas Sci. Eng.* **2010**, *2*, 49–59. [CrossRef]
5. Li, J.; Ye, J.; Qin, X.; Qiu, H.; Wu, N.; Lu, H.; Xie, W.; Lu, J.; Peng, F.; Xu, Z.; et al. The first offshore natural gas hydrate production test in South China Sea. *China Geol.* **2018**, *1*, 5–16. [CrossRef]
6. Yan, C.; Li, Y.; Chen, Y.; Wang, W.; Song, B.; Deng, F.; Feng, Y. Sand production evaluation during gas production from natural gas hydrates. *J. Nat. Gas Sci. Eng.* **2018**, *57*, 77–88. [CrossRef]
7. Pan, D.; Zhong, X.; Zhu, Y.; Zhai, L.; Zhang, H.; Li, X.; Wang, Y.; Chen, C. $CH_4$ recovery and $CO_2$ sequestration from hydrate-bearing clayey sediments via $CO_2$/$N_2$ injection. *J. Nat. Gas Sci. Eng.* **2020**, *83*, 103503. [CrossRef]
8. Chen, C.; Yang, L.; Jia, R.; Sun, Y.; Guo, W.; Chen, Y.; Li, X. Simulation Study on the Effect of Fracturing Technology on the Production Efficiency of Natural Gas Hydrate. *Energies* **2017**, *10*, 1241. [CrossRef]

9. Lim, J.; Kim, E.; Seo, Y. Dual inhibition effects of diamines on the formation of methane gas hydrate and their significance for natural gas production and transportation. *Energy Convers. Manag.* **2016**, *124*, 578–586. [CrossRef]
10. Li, G.; Moridis, G.J.; Zhang, K.; Li, X.-S. Evaluation of Gas Production Potential from Marine Gas Hydrate Deposits in Shenhu Area of South China Sea. *Energy Fuels* **2010**, *24*, 6018–6033. [CrossRef]
11. Boswell, R.; Collett, T.S. Current perspectives on gas hydrate resources. *Energy Environ. Sci.* **2011**, *4*, 1206–1215. [CrossRef]
12. Lee, Y.; Choi, W.; Shin, K.; Seo, Y. $CH_4$–$CO_2$ replacement occurring in sII natural gas hydrates for $CH_4$ recovery and $CO_2$ sequestration. *Energy Convers. Manag.* **2017**, *150*, 356–364. [CrossRef]
13. Wang, Y.; Feng, J.; Li, X.; Zhang, Y. Experimental investigation of optimization of well spacing for gas recovery from methane hydrate reservoir in sandy sediment by heat stimulation. *Appl. Energy* **2017**, *207*, 562–572. [CrossRef]
14. Zheng, R.; Li, S.; Li, X. Sensitivity analysis of hydrate dissociation front conditioned to depressurization and wellbore heating. *Mar. Pet. Geol.* **2018**, *91*, 631–638. [CrossRef]
15. Zhang, G.; Ma, X.; Jiang, D.; Lu, J.; Fang, X.; Pan, D. Characteristics of hydrate formation, decomposition, and phase equilibrium in the transition area formed by the high-pressure jet breaking and sand filling method. *Energy Rep.* **2022**, *8*, 312–321. [CrossRef]
16. Zhong, X.; Pan, D.; Zhu, Y.; Wang, Y.; Tu, G.; Nie, S.; Ma, Y.; Liu, K.; Chen, C. Commercial production potential evaluation of injection-production mode for CH-Bk hydrate reservoir and investigation of its stimulated potential by fracture network. *Energy* **2022**, *239*, 122113. [CrossRef]
17. Chong, Z.R.; Yang, S.H.B.; Babu, P.; Linga, P.; Li, X.-S. Review of natural gas hydrates as an energy resource: Prospects and challenges. *Appl. Energy* **2016**, *162*, 1633–1652. [CrossRef]
18. Wang, B.; Huo, P.; Luo, T.; Fan, Z.; Liu, F.; Xiao, B.; Yang, M.; Zhao, J.; Song, Y. Analysis of the Physical Properties of Hydrate Sediments Recovered from the Pearl River Mouth Basin in the South China Sea: Preliminary Investigation for Gas Hydrate Exploitation. *Energies* **2017**, *10*, 531. [CrossRef]
19. Wang, X.; Li, F.; Xu, Y.; Sun, C.; Pan, H.; Liu, B.; Yang, L.; Chen, G.; Li, Q. Elastic properties of hydrate-bearing sandy sediment during $CH_4$–$CO_2$ replacement. *Energy Convers. Manag.* **2015**, *99*, 274–281. [CrossRef]
20. Sun, J.; Zhang, L.; Ning, F.; Lei, H.; Liu, T.; Hu, G.; Lu, H.; Lu, J.; Liu, C.; Jiang, G.; et al. Production potential and stability of hydrate-bearing sediments at the site GMGS3-W19 in the South China Sea: A preliminary feasibility study. *Mar. Pet. Geol.* **2017**, *86*, 447–473. [CrossRef]
21. Lin, J.-S.; Uchida, S.; Myshakin, E.M.; Seol, Y.; Rutqvist, J.; Boswell, R. Assessing the geomechanical stability of interbedded hydrate-bearing sediments under gas production by depressurization at NGHP-02 Site 16. *Mar. Pet. Geol.* **2018**, *108*, 648–659. [CrossRef]
22. Jang, J.; Waite, W.F.; Stern, L.A.; Collett, T.S.; Kumar, P. Physical property characteristics of gas hydrate-bearing reservoir and associated seal sediments collected during NGHP-02 in the Krishna-Godavari Basin, in the offshore of India. *Mar. Pet. Geol.* **2018**, *108*, 249–271. [CrossRef]
23. Oyama, H.; Konno, Y.; Suzuki, K.; Nagao, J. Depressurized dissociation of methane-hydrate-bearing natural cores with low permeability. *Chem. Eng. Sci.* **2012**, *68*, 595–605. [CrossRef]
24. Konno, Y.; Oyama, H.; Nagao, J.; Masuda, Y.; Kurihara, M. Numerical Analysis of the Dissociation Experiment of Naturally Occurring Gas Hydrate in Sediment Cores Obtained at the Eastern Nankai Trough, Japan. *Energy Fuels* **2010**, *24*, 6353–6358. [CrossRef]
25. Zhong, X.; Pan, D.; Zhai, L.; Zhu, Y.; Zhang, H.; Zhang, Y.; Wang, Y.; Li, X.; Chen, C. Evaluation of the gas production enhancement effect of hydraulic fracturing on combining depressurization with thermal stimulation from challenging ocean hydrate reservoirs. *J. Nat. Gas Sci. Eng.* **2020**, *83*, 103621. [CrossRef]
26. Wang, B.; Dong, H.; Liu, Y.; Lv, X.; Liu, Y.; Zhao, J.; Song, Y. Evaluation of thermal stimulation on gas production from depressurized methane hydrate deposits ☆. *Appl. Energy* **2018**, *227*, 710–718. [CrossRef]
27. Zhao, J.; Wang, J.; Liu, W.; Song, Y. Analysis of heat transfer effects on gas production from methane hydrate by thermal stimulation. *Int. J. Heat Mass Transf.* **2015**, *87*, 145–150. [CrossRef]
28. Selim, M.; Sloan, E. Heat and mass transfer during the dissociation of hydratesin porous media. *AIChE* **1989**, *35*, 1049–1052. [CrossRef]
29. Yuan, Q.; Sun, C.-Y.; Liu, B.; Wang, X.; Ma, Z.-W.; Ma, Q.-L.; Yang, L.-Y.; Chen, G.-J.; Li, Q.-P.; Li, S.; et al. Methane recovery from natural gas hydrate in porous sediment using pressurized liquid CO2. *Energy Convers. Manag.* **2013**, *67*, 257–264. [CrossRef]
30. Yang, J.; Okwananke, A.; Tohidi, B.; Chuvilin, E.; Maerle, K.; Istomin, V.; Bukhanov, B.; Cheremisin, A. Flue gas injection into gas hydrate reservoirs for methane recovery and carbon dioxide sequestration. *Energy Convers. Manag.* **2017**, *136*, 431–438. [CrossRef]
31. Chen, Y.; Gao, Y.; Zhao, Y.; Chen, L.; Dong, C.; Sun, B. Experimental investigation of different factors influencing the replacement efficiency of $CO_2$ for methane hydrate. *Appl. Energy* **2018**, *228*, 309–316. [CrossRef]
32. Demirbas, A. Methane hydrates as potential energy resource: Part 1—Importance, resource and recovery facilities. *Energy Convers. Manag.* **2010**, *51*, 1547–1561. [CrossRef]
33. Demirbas, A. Methane hydrates as potential energy resource: Part 2—Methane production processes from gas hydrates. *Energy Convers. Manag.* **2010**, *51*, 1562–1571. [CrossRef]
34. Koh, D.-Y.; Kang, H.; Lee, J.-W.; Park, Y.; Kim, S.-J.; Lee, J.; Lee, J.Y.; Lee, H. Energy-efficient natural gas hydrate production using gas exchange. *Appl. Energy* **2016**, *162*, 114–130. [CrossRef]

35. Ye, J.; Qin, X.; Qiu, H.; Liang, Q.; Dong, Y.; Wei, J.; Lu, H.; Lu, J.; Shi, Y.; Zhong, C.; et al. Preliminary results of environmental monitoring of the natural gas hydrate production test in the South China Sea. *China Geol.* **2018**, *1*, 202–209. [CrossRef]
36. Zhou, S.; Zhao, J.; Li, Q.; Chen, W.; Zhou, J.; Wei, N.; Guo, P.; Sun, W. Optimal design of the engineering parameters for the first global trial production of marine natural gas hydrates through solid fluidization. *Nat. Gas Ind. B* **2018**, *5*, 118–131. [CrossRef]
37. Li, Y.; Cao, G. Development technology for low-permeability sandstone reservoirs in Shengli Oil field. *Pet. Explor. Dev.* **2005**, *32*, 123–126. [CrossRef]
38. Zhang, Y.J.; Li, Z.W.; Guo, L.L.; Gao, P.; Jin, X.P.; Xu, T.F. Electricity generation from enhance geothermal systems by oilfield produced water circulating through reservoir stimulated by staged fracturing technology for horizontal wells: A case study in Xujiaweizi area in Daqing Oilfield, China. *Energy* **2014**, *78*, 788–805. [CrossRef]
39. Wang, G.; Huang, R.; Zhong, L.; Wang, Z.; Zhou, S.; Liu, Q. An optimal design of crushing parameters of Marine gas hydrate reservoirs in solid fluidization exploitation. *Nat. Gas Ind.* **2018**, *38*, 84–89. [CrossRef]
40. Tang, Y.; Sun, P.; Wang, G.; Fu, B.; Yao, J. Rock-breaking mechanism and efficiency of straight-swirling mixed nozzle for the nondiagenetic natural gas hydrate in deep-sea shallow. *Energy Sci. Eng.* **2020**, *8*, 3740–3752. [CrossRef]
41. Wang, L.; Wang, G. Experimental and Theoretical Study on the Critical Breaking Velocity of Marine Natural Gas Hydrate Sediments Breaking by Water Jet. *Energies* **2020**, *13*, 1725. [CrossRef]
42. Chen, C.; Pan, D.; Yang, L.; Zhang, H.; Li, B.; Jin, C.; Li, X.; Cheng, Y.; Zhong, X. Investigation into the Water Jet Erosion Efficiency of Hydrate-Bearing Sediments Based on the Arbitrary Lagrangian-Eulerian Method. *Appl. Sci.* **2019**, *9*, 182. [CrossRef]
43. Jichun, Z.; Lin, Z.; Guorong, W. Experimental study on crushing law of single jet for non-diagenetic gas hydrate. *J. Cent. South Univ. Sci. Technol.* **2021**, *52*, 607–613.
44. Liu, T.; Zhou, L.; Kou, H.; Zhang, M. Model test of stratum failure and pore pressure variation induced by THF hydrate dissociation. *Mar. Georesour. Geotechnol.* **2018**, *37*, 539–546. [CrossRef]
45. Lee, J.Y.; Santamarina, J.C.; Ruppel, C. Mechanical and electromagnetic properties of northern Gulf of Mexico sediments with and without THF hydrates. *Mar. Pet. Geol.* **2008**, *25*, 884–895. [CrossRef]
46. Zhang, X.; Lu, X.; Shi, Y.; Xia, Z.; Liu, W. Centrifuge experimental study on instability of seabed stratum caused by gas hydrate dissociation. *Ocean. Eng.* **2015**, *105*, 1–9. [CrossRef]
47. Zhang, X.; Lu, X.; Wang, S.; Li, Q. Experimental study of static and dynamic properties of tetrahydrofuran hydrate-bearing sediments. *Rock Soil Mech.* **2010**, *32*, 303–308.
48. Sun, S.; Peng, X.; Zhang, Y.; Zhao, J.; Kong, Y. Stochastic nature of nucleation and growth kinetics of THF hydrate. *J. Chem. Thermodyn.* **2017**, *107*, 141–152. [CrossRef]
49. Liu, W.; Wang, S.; Yang, M.; Song, Y.; Wang, S.; Zhao, J. Investigation of the induction time for THF hydrate formation in porous media. *J. Nat. Gas Sci. Eng.* **2015**, *24*, 357–364. [CrossRef]
50. Momber, A.W. Deformation and fracture of rocks due to high-speed liquid impingement. *Int. J. Fract.* **2004**, *130*, 683–704. [CrossRef]
51. Yanaida, K.; Ohashi, A. Flow characteristics of water jets. In Proceedings of the Second International Symposium on Jet Cutting Technology, Cambridge, UK, 2–4 April 1974; p. A2.
52. Li, X.; Lu, Y.; Xiang, W. *Water Jet Theory and Its Application in Mining Engineering*; Chongqing University Press: Chongqing, China, 2007. (In Chinese)
53. Rajaratnam, N. Turbulent Jets. *Dev. Water Sci.* **1976**, *5*, 77–82.
54. Sen, T.K.; Mahajan, S.; Khilar, K.C. Colloid-Associated contaminant transport in porous media: 1. Experimental studies. *AIChE J.* **2002**, *48*, 2366–2374. [CrossRef]
55. Pandya, V.B.; Bhuniya, S.; Khilar, K.C. Existence of a critical particle concentration in plugging of a packed bed. *Am. Inst. Chem. Eng. AIChE J.* **1998**, *44*, 978. [CrossRef]